A Combined Spectroscopic and Theoretical Study of Dibutyltin Diacetate and Dilaurate in Supercritical CO_2

Benjamin Renault,[†,‡] Eric Cloutet,[†] Henri Cramail,[†] Yacine Hannachi,[‡] and Thierry Tassaing*[,‡]

Laboratoire de Chimie des Polymères Organiques, ENSCPB-CNRS-Université Bordeaux 1 (UMR 5629), 16 Avenue Pey-Berland, 33607 Pessac cedex, France, and Institut des Sciences Moléculaires, CNRS-Université Bordeaux 1 (UMR 5255), 351, Cours de la Libération, 33405 Talence cedex, France

Received: January 23, 2008; Revised Manuscript Received: June 18, 2008

Two organotin catalysts, namely, dibutyltin dilaurate (DBTDL) and dibutyltin diacetate (DBTDA), commonly used in the synthesis of polyurethanes, have been investigated combining vibrational spectroscopic measurements with molecular modeling. The structure and vibrational spectra of the DBTDA molecule have been simulated using density functional theory. Thus, because of the Sn···O interactions, the lowest energy conformer reveals an asymmetrically chelated structure of the acetate groups with a C_{2v} symmetry. The experimental IR spectra of DBTDA and DBTDL diluted in carbon tetrachloride and in supercritical CO_2 show unambiguously that these molecules adopt the asymmetrically chelated conformation in the solvent. A new attribution of the main peaks constituting the respective IR spectra of the catalysts could be carried out. Finally, from the IR spectra of the two catalysts diluted in supercritical CO_2 reported as a function of time, it was found that both molecules react slightly with CO_2. However, their spectrum remains unchanged at the earliest stage of the polymerization, indicating that these molecules preserve a catalytic activity similar to that noted in conventional organic solvent.

1. Introduction

Polyurethanes were first made in 1937 by Otto Bayer at I. G. Farben by developing the novel polyisocyanate-polyaddition process.[1] They are now defined by the Alliance for the Polyurethanes Industry (API) as "polymers formed by reacting a polyol with a diisocyanate or a polymeric isocyanate in the presence of suitable catalysts and additives." Although tertiary amines catalyze such reactions,[2] organotin compounds, and more specifically diorganotin(IV) ester compounds (e.g., dibutyltin dilaurate (DBTDL), dibutyltin diacetate (DBTDA), and dibutyltin bis(2-ethylhexanoate)), exhibit remarkably high catalytic activity and are commonly used in the industrial production of polyurethanes. Diorganotin dicarboxylates have been the subject of numerous experimental studies. Conflicting theories on the way they catalyze alcohol−isocyanate reactions have been put forth, and the debate is still very active.[3−12] To better understand their unique catalytic efficiency, some investigations have been reported about the molecular structure and conformation of such compounds.[13−16] While the first description of dialkyltin diacetates was given by Cahours in 1860,[13] the FTIR spectra of DBTDA were reported later in 1967 by Okawara et al.[14,15] These authors pointed out the nonsymmetrically chelated octahedral configuration of the catalyst in diluted benzene solutions (Figure 1a) and the partial bridging of the acetoxy group at higher concentrations (Figure 1b). More recently, besides the renewed interest in organotin complexes in the field of organometallic chemistry,[17] diorganotin compounds were mostly investigated in the context of their biological activity and their antitumor potential.[18−21]

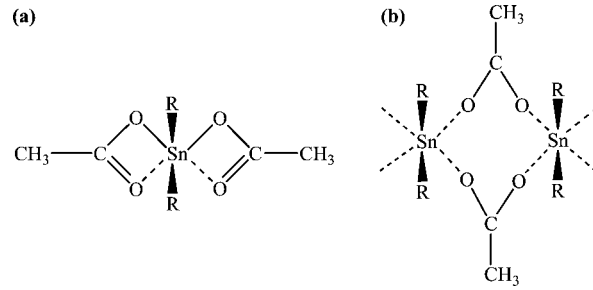

Figure 1. Structures of dialkyltin diacetate according to Okawara et al.[14,15]

Supercritical carbon dioxide ($scCO_2$) has received much attention within academic and chemical industrial laboratories as a "green" alternative to conventional organic solvents and has newly emerged as a promising medium for polymerization reactions. In this context, we have recently investigated the synthesis of polyurethanes by polyaddition between a short aliphatic diol (e.g., ethylene glycol or 1,4-butanediol) and an aromatic diisocyanate (i.e., tolylene-2,4-diisocyanate) in the presence of DBTDL as a catalyst in both, cyclohexane and $scCO_2$, used as dispersant media.[22−25] In these investigations, $scCO_2$ was found quite attractive, not only as a neat substitute of organic media for dispersion polymerizations, but also as a unique way to synthesize high molecular weight polyurethane materials using only low molecular weight monomers and diorgatin dicarboxylates as catalysts. However, several studies revealed that the behavior of organotin compounds may be affected when $scCO_2$ is used as the solvent, indicating the necessity of a close examination of the nature of the interaction occurring in such a system. Indeed, Stassin et al.[26] observed that the polymerization of ε-caprolactone initiated by a tin alkoxide (i.e., tin dibutyldimethoxide) was much faster in a conventional organic medium (e.g., in toluene) than in $scCO_2$,

* To whom correspondence should be addressed. E-mail: t.tassaing@ism.u-bordeaux1.fr. Tel: +33540002892. Fax: +33540008402.
† ENSCPB-CNRS-Université Bordeaux 1 (UMR 5629).
‡ CNRS-Université Bordeaux 1 (UMR 5255).

10.1021/jp8004822 CCC: $40.75
Published on Web 08/15/2008

postulating that a coordination of CO_2 onto the metal of the initiator may happen and slow the reaction. A similar observation has been reported by Bergeot et al.[27] for anionic ring opening polymerization of ε-caprolactone in $scCO_2$ using different metal alkoxides (i.e., $Y(OiPr)_3$, $La(OiPr)_3$, and $Al(OiPr)_3$). They noticed that carbonates formed from the reaction between ionic alkoxides and CO_2 lead to a strong decrease of the polymerization rate compared with that carried out in regular solvents. In this context, it was essential to check if such reactions that modify the activity of organotin compounds may occur (or not) between CO_2 and the diorganotin compounds that we have used in our polymerization, namely, DBTDA and DBTDL. Besides, to the best of our knowledge, the structure and vibrational spectra of diorganotin dicarboxylates compounds have never been studied in detail, in particular using quantum calculations. All these considerations prompted us to investigate by means of vibrational spectroscopy and Density Functional Theory (DFT) calculations, the molecular structure and the vibrational spectra of DBTDL and DBTDA, and to compare the behavior of both catalysts diluted either in $scCO_2$ or liquid carbon tetrachloride. In view of the size of the DBTDL molecule, the DFT calculations have been performed only for DBTDA.

The first part of the paper displays a detailed analysis of the molecular structure and the vibrational spectra of DBTDA. In particular, the relative energies and the relevant frequencies of the different conformers of DBTDA monomer with respect to the relative orientation of the two carboxylate functions are reported. Solvents effects were also included to probe the influence of the solvent on the relative stability of the different conformers and take it into account in the calculation of their structure and vibrational spectra. The next part of the article is devoted to the mid infrared absorption (IR) and Raman scattering measurements on DBTDA and DBTDL diluted in CCl_4 and in $scCO_2$. Because of their low solubility, these organotin compounds can not be detected by Raman spectroscopy once diluted in $scCO_2$, and only the IR spectra were recorded in such conditions. In particular, we paid attention to the C═O oscillator of DBTDA and DBTDL in order to probe the intermolecular interactions between each catalyst and CO_2, and check that their catalytic activity is little or not altered.

2. Experimental Details

The IR measurements were performed on a Biorad interferometer (type FTS-60A) equipped with a globar source, a Ge/KBr beam splitter and a DTGS detector. Single beam spectra recorded in the spectral range 400−6000 cm^{-1} with a 2 cm^{-1} resolution were obtained by Fourier transformation of 50 accumulated interferograms. To collect the IR spectra of the catalysts diluted in liquid organic solvents, we have used a standard liquid cell equipped with KRS5 windows. For measurements in $scCO_2$, we have used a stainless steel cell, equipped with four cylindrical windows, two silicium windows for the infrared absorption measurements with a path length of 25 mm (that can be varied from 3 to 25 mm) and two sapphire windows for direct observation of the solution. Details about the cell and control of pressure and temperature have been given elsewhere.[28] The cell was filled with DBTDA or DBTDL respectively (Aldrich products, 98% purity) and heated up to the required temperature. Carbon dioxide (CO_2, from the "Air Liquide" company) was then added up to the desired pressure.

The Raman spectra were collected on a DILOR Labram confocal spectrograph equipped with a CCD detector. The source was a Spectra Physics argon−krypton laser operating at a wavelength of 514.5 nm with a power of 300 mW. The spectra were recorded using a back scattering geometry at 3 cm^{-1} resolution with an accumulation time of 100 s.

TABLE 1: Calculated Relative Energies (kcal/mol) of the Different Conformers of DBTDA at the B3LYP and MP2 Level of Theory in the Gas Phase and at the B3LYP in CCl_4 Solution

structure	ΔE_0 (B3LYP)	ΔE_0 (MP2)	ΔE_0 (B3LYP) in CCl_4
1	0.0	0.0	0.0
2	2.9	3.0	2.9
3	2.9	3.0	3.0
4	12.2	13.5	10.4
5	12.3	14.1	10.6
6	14.0	19.4	11.8
7	30.1	33.5	26.2

3. Computational Details

Density functional calculations were carried out using the Gaussian 03 program suite[29] with the popular hybrid B3LYP functional.[30−32] The geometry optimization was achieved using a polarized valence double-ζ basis set as implemented in DGauss program (named DGDZVP in Gaussian program).[33,34] Geometry computation was not subjected to any symmetry constraint. When a particular symmetry was obtained, the geometry was reoptimized under the desired symmetry. Single-point energy calculation was achieved at the MP2 level (frozen core) with the same basis set at the B3LYP optimized geometry for sake of comparison. All reported relative energies have been corrected for zero-point vibrational energy obtained at the B3LYP level. Vibrational analyses were carried out within the standard Wilson FG matrix formalism from the appropriate optimized structures of DBTDA at the B3LYP/DGDZVP level of calculations. Molden was used to display the optimized geometry and the vibrational modes.[35] The calculated frequency values were corrected using standard scaling factors available from literature to allow a comparison with the experimental ones.[36,37] In the present case, we used a scaling factor of 0.96.

To assess the solvent effects on the relative stability and vibrational spectra of the different conformers of DBTDA, we reoptimized the various structures using the polarizable continuum model (PCM)[38−40] with carbon tetrachloride as solvent, which has a dielectric constant ε of 2.228. Let us emphasize that the dielectric constant of $scCO_2$, which depends upon the temperature and the pressure,[41] is always lower in our conditions (ε = 1.5 at 60 °C and 30 MPa) than that of liquid CCl_4.

4. Results and Discussion

4.1. Analysis of the DBTDA Structure from DFT Calculations. Many different starting structures were used for geometry optimization. We tested nonchelated structure, structures with only one chelated acetate moieties (either symmetric or asymmetric), and with both acetate moieties chelated. Although different rotamers with respect to the C−C bonds of the butyl groups might be generated, only the lowest energy ones were considered. Seven different minima were located. The calculated relative energies of the different conformers obtained at the B3LYP and MP2 level are reported in Table 1. The agreement between the two theoretical approaches is very good, taking into account that MP2 energies were obtained at the B3LYP optimized geometries. No symmetrically chelated species could be obtained ($SnO_a \neq SnO_b$ and $SnO_c \neq SnO_d$, see Figures 2 and 3). The main difference between the obtained structures is the relative orientation of the two acetate groups

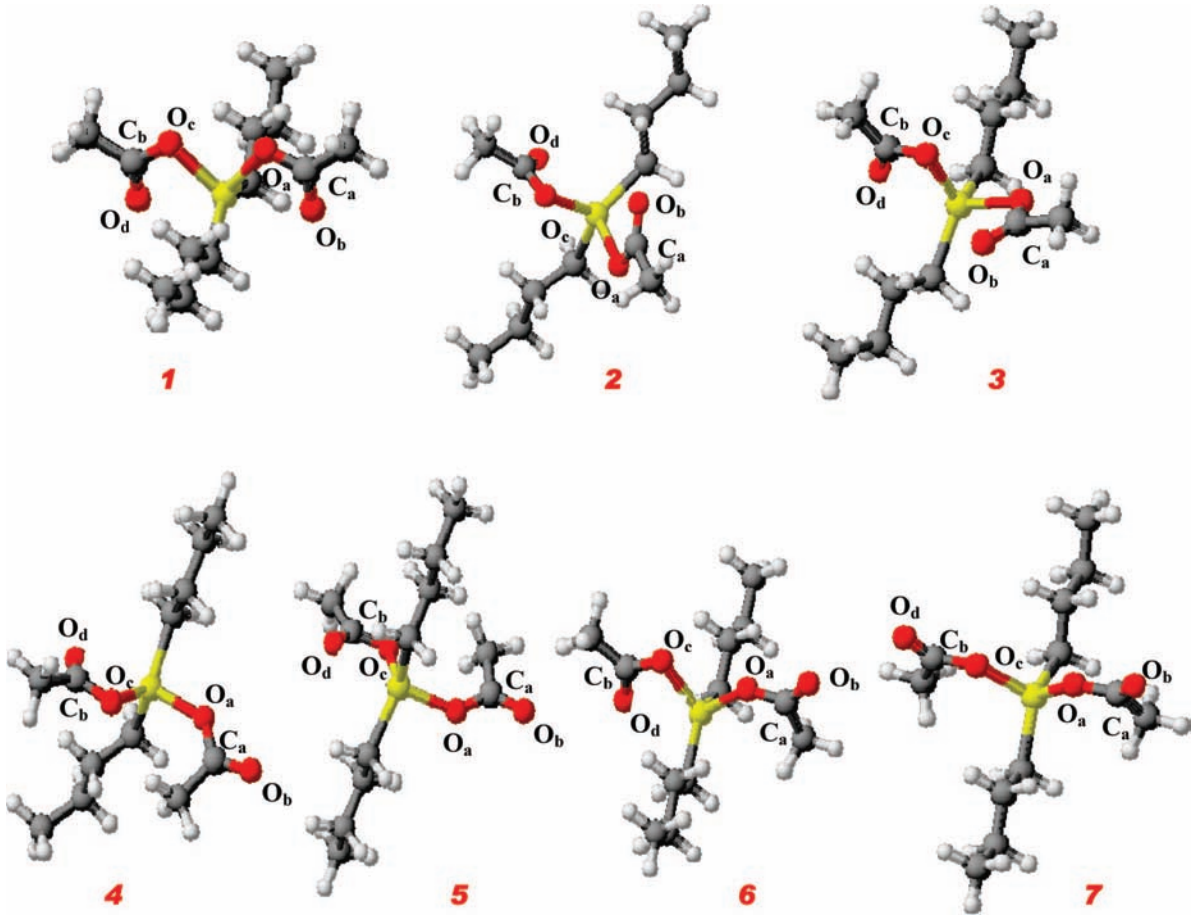

Figure 2. Optimized geometries of DBTDA obtained at the B3LYP/DGDZVP level.

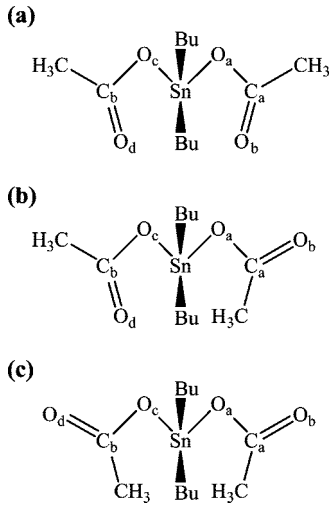

Figure 3. Schematic representations of the different types of optimized geometries of DBTDA.

(see Figures 2 and 3). The seven conformers can be classified as either asymmetrically chelated on both sides (structures **1**−**3** (a)), asymmetrically chelated just on one side (structures **4**−**6** (b)) or nonchelated on both sides (structure **7** (c)) (Figures 2 and 3). The difference in the relative stability of the various located minima is directly related to the orientation of the terminal oxygen atoms toward Sn atom, suggesting that both of the terminal oxygen atoms interact with the tin atom. Indeed, the lowest energy conformers (structures **1** to **3**) have the two terminal oxygen atoms pointing toward the tin atom, displaying SnOCO dihedral angles equal or close to 0° (Table 2). About 12 kcal·mol^{-1} higher in energy, structures **4** to **6** exhibit only one terminal oxygen pointing in the direction of the tin atom with one SnOCO dihedral angle close to zero and the other one close to 180° (Figure 3b). The highest energy conformer shows both terminal oxygens pointing in the opposite direction with both SnOCO dihedral angles close to 180° (Figure 3c).

The two acetate groups of the lowest energy conformer (structure **1**, Figure 2) display rigorously identical chelated geometries. The overall symmetry of the absolute minimum is C_{2v}. The two SnO and the two CO bond lengths are respectively quite different within a Sn−Ac fragment, indicating an asymmetrically chelated structure (2.15/2.60 Å and 1.31/1.25 Å for SnO and CO bonds, respectively, (Table 2)). However, although the two CO bonds constituting each of the acetate groups might be characterized as one double and one single bond, a weak electron delocalization of the π system can be noticed. Indeed, the typical C═O double bond length in (formaldehyde) H_2CO is about 1.21 Å and the typical C−O single bond in methanol (CH_3OH) is about 1.43 Å at B3LYP/DGDZVP. The $O_cSnO_aC_a$ dihedral angle is strictly equal to 0°. Despite structures **2** and **3** being similar to structure **1**, the geometries of the two acetate groups are not strictly identical. On the one hand, the Sn−O_a bond is shortened to some extent whereas the Sn···O_b bond is markedly lengthened. This has the effect to shorten the C_a═O_b bond and to stretch the C_a−O_a one with respect to structure **1**. On the other hand, the Sn−O_c is virtually unchanged with respect to structure **1** whereas the Sn···O_d undergoes a slight shortening. Thus, the length of the C_b−O_c bond remains the same while the C_b═O_d bond is slightly lengthened. As mentioned above, the main difference between structures **2** and **3** results remains in the relative orientation of their two acetate

TABLE 2: Calculated Relevant Geometrical Parameters of the Different Conformers of DBTDA

	dihedral angle (deg)		interatomic distances (Å)							
structure	$SnO_aC_aO_b$	$SnO_cC_bO_d$	Sn−O_a	Sn···O_b	C_a−O_a	C_a−O_b	Sn−O_c	Sn···O_d	C_b−O_c	C_b−O_d
1	0	0	2.147	2.597	1.308	1.249	2.147	2.597	1.308	1.249
2	∼0	∼0	2.111	2.920	1.325	1.233	2.141	2.506	1.304	1.253
3	∼0	∼0	2.111	2.920	1.325	1.233	2.141	2.506	1.304	1.253
4	174	∼0	2.061	4.249	1.344	1.218	2.150	2.510	1.307	1.252
5	150	∼0	2.055	4.220	1.344	1.218	2.153	2.507	1.307	1.252
6	∼180	∼0	2.066	4.242	1.338	1.218	2.127	2.516	1.307	1.252
7	∼180	∼180	2.038	4.203	1.347	1.214	2.038	4.203	1.347	1.214

TABLE 3: Relevant Infrared Frequencies (in cm^{-1}) and IR Intensities (in km/mol) of Structure 1 of DBTDA Obtained at the DFT/DGDZVP

assignments[a]	frequency (cm^{-1})	IR intensity (km/mol)
C_aO_b + C_bO_d i.p. str	1596	386
C_aO_b + C_bO_d op str	1582	7
C_aO_a + C_bO_c i.p. str + CH_3 sym def	1384	2
C_aO_a + C_bO_c o.p. str + CH_3 sym def	1375	468
C_aO_a + C_bO_c i.p. str + CH_3 sym def	1322	6
C_aO_a + C_bO_c o.p. str + CH_3 sym def	1315	238
CH_2 butyl chains rock	663	154

[a] i.p. = in phase; o.p. = out of phase; str = stretch; sym = symmetric; def = deformation.

TABLE 4: Relevant IR Frequencies and Intensities of Structures 2 and 3 of DBTDA Obtained at the DFT/DGDZVP

	structure **2**		structure **3**	
assignments[a]	frequency (cm^{-1})	IR intensity (km/mol)	frequency (cm^{-1})	IR intensity (km/mol)
C_aO_b str	1648	287	1647	287
C_bO_d str	1575	218	1574	219
CH_3 sym def + C_bO_c str.	1387	224	1387	223
CH_3 sym def + C_aO_a str.	1356	128	1356	128
CH_3 sym def + C_bO_c str.	1326	62	1326	62
CH_3 sym def + $C_aO_a$str.	1278	228	1278	229
CH_2 butyl chains rock	660	74	660	74

[a] i.p. = in phase; o.p. = out of phase; str = stretch; sym = symmetric; def = deformation.

groups, displaying respectively $O_cSnO_aC_a$ dihedral angles of about −70° and 70°.

As revealed by the calculated Sn−O_b bond distances and $SnO_aC_aO_b$ dihedral angles, structures **4**−**6** have only one asymmetrically chelated acetate moiety (Table 2). In comparison to structures **1**−**3**, the Sn−O_a bond lengths are slightly shortened whereas the C_a−O_a bonds are lengthened. The terminal C═O bond length (C_a═O_b) of the nonchelated acetate moiety is close to that of a typical double bond. As in the case of structures **2** and **3**, the major distinction between structures **4**, **5**, and **6** is illustrated by the respective values of $O_cSnO_aC_c$ dihedral angles of about 56°, −63°, and 180°.

Finally, the highest energy conformer, that is, structure **7**, is very close to C_{2v} symmetry. Attempt to optimize it under a C_{2v} symmetry constraint resulted in a small imaginary frequency. Acetate moieties are both nonchelated. For this reason, this conformer displays the shortest Sn−O (Sn−O_a and Sn−O_c) bond (2.038 Å), and the lengths of the terminal C_a═O_b and C_b═O_d bonds are much closer to a typical double bond.

When carbon tetrachloride is taken into account as a solvent using the polarizable continuum model, the energetic order of the different conformers of DBTDA is unchanged as shown in Table 1. The relative energies of conformers **2** and **3** are virtually unchanged with respect of gas phase values. This is not surprising since their calculated dipole moment in the gas phase (1.5 D) is close to that of conformer **1** (0.5 D). Conformers **4**−**6** are stabilized by about 2 kcal/mol since their calculated gas phase dipole moment is of about 6 Debyes. Conformer **7** is stabilized by about 4 kcal/mol as its calculated gas phase dipole moment is about 10 D. Finally, we notice that the structural parameters of the different conformers are virtually unchanged in carbon tetrachloride solvent with respect to gas phase values.

4.2. Calculated Vibrational Spectra. Tables 3−6 report the calculated vibrational frequencies together with IR intensities. As the number of vibrational modes is large, only those involving CO stretches, which are in the fingerprint region together with the calculated most intense bands, are reported. The CH-stretching region is not discussed as well since it is not needed to discriminate the different conformers. Since, in a given vibrational mode, a coupling might exist between many internal motions, only the most predominant ones are mentioned unless the coupling is significant. The vibrational modes of the lowest energy conformer are reported in Table 3. The C_a═O_b and C_b═O_d bonds (Figures 2 and 3) are equivalent and thus coupled resonantly. The symmetric stretch, at 1596 cm^{-1}, is calculated as quite intense with an IR intensity of 386 km/mol. The asymmetric one, at 1582 cm^{-1}, is predicted to be much less intense (7 km/mol) and should be difficult to observe. The two equivalent C_a−O_a and C_b−O_c stretches are both coupled with the CH_3-symmetric deformation motions of the acetate groups. They give rise to a set of four vibrational modes in the 1200−1400 frequency range. The asymmetric modes, calculated at 1375 and 1315 cm^{-1}, are intense (468 and 238 km/mol, respectively) while the symmetric ones are much less active. The latter are calculated at 1384 and 1322 cm^{-1} with IR intensities of 2 and 6 km/mol, respectively. Finally, a band corresponding to the asymmetric rock of the CH_2 groups of the butyl chains is expected at 663 cm^{-1} with an IR intensity of 154 km/mol.

Table 4 reports the relevant vibrational frequencies and IR intensities of structures **2** and **3**. The characteristic frequencies of the two conformers are roughly identical, which is not surprising since the structural parameters are very similar (besides the mutual orientation of the two acetate groups). However, the nature of the vibrational and coupling modes involved in these structures is significantly different from those observed in structure **1**. Because of the asymmetry of the overall geometry, the vibrational motion of the two acetate groups does not couple. The highest C═O frequency is obtained around 1648 cm^{-1} which corresponds to the stretching of the C_a═O_b bond, in agreement with the calculated bond lengths. Its estimated IR intensity is 287 km/mol. The stretch of the C_b═O_d bond is predicted at about 1575 cm^{-1} with an IR intensity of about 220 km/mol. The C_a−O_a and C_b−O_c stretching motions are coupled with their respective neighboring CH_3 symmetric deformations. This results in a set of four distinct vibrational modes in the

TABLE 5: Relevant IR Frequencies and Intensities of Structures 4 to 6 of DBTDA Obtained at the DFT/DGDZVP

	structure **4**		structure **5**		structure **6**	
assignments[a]	frequency (cm^{-1})	IR intensity (km/mol)	frequency (cm^{-1})	IR intensity (km/mol)	frequency (cm^{-1})	IR intensity (km/mol)
C_aO_b str	1707	504	1703	483	1707	508
C_bO_d str	1576	221	1578	221	1577	202
CH_3 sym def + C_bO_c str	1381	243	1380	256	1384	210
CH_3 sym def + C_bO_c str	1322	83	1322	95	1324	67
C_aO_a str	1223	537	1224	540	1229	549
CH_2 butyl chains rock	665	63	667	94	662	70

[a] i.p. = in phase; o.p. = out of phase; str = stretch; sym = symmetric; def = deformation.

TABLE 6: Relevant IR Frequencies and Intensities of Structure 7 of DBTDA Obtained at the DFT/DGDZVP

assignments[a]	frequency (cm^{-1})	IR intensity (km/mol)
C_aO_b+C_bO_d i.p. str	1727	474
C_aO_b+C_bO_d o.p. str	1719	506
o.p. CH_3 sym def	1346	93
C_aO_a+C_bO_c i.p. str	1225	≈ 0
C_aO_a+C_bO_c o.p. str	1200	1054
CH_3 (Ac) o.p. // rock	972	161
CH_2 butyl chains rock	659	52

[a] i.p. = in phase; o.p. = out of phase; str = stretch; sym = symmetric; def = deformation; // = parallel.

1200−1400 frequency range, with non-negligible IR intensities. The vibrational modes involving the C_a-O_a stretch are calculated at 1356 and 1278 cm^{-1} with IR intensities of about 128 and 228 km/mol whereas those involving the C_b-O_c are determined at 1387 and 1326 cm^{-1} with IR intensities of about 224 and 62 km/mol respectively. Finally, a last relevant band, corresponding to the CH_2 chain rock, is predicted at 660 cm^{-1} with an IR intensity of 74 km/mol.

As in the case of the conformers **2** and **3**, the calculated relevant frequencies of the conformers **4**, **5**, and **6** are very similar (see Table 5). The $C_a=O_b$ stretching mode, not involved in a chelated structure, is found above 1700 cm^{-1}, with an intensity around 500 km/mol. Because of the interaction occurring between O_d and the tin atom, the $C_b=O_d$ stretching mode logically appears at a lower frequency around 1577 cm^{-1} with an IR intensity about 220 km/mol, as observed in structures **2** and **3**. The C_b-O_c stretching motion couples with the neighboring CH_3 symmetric deformation of the acetate group, which gives rise to two intense bands respectively located at about 1381 and 1322 cm^{-1}. More noteworthy, the C_a-O_a stretch is only weakly coupled to the CH_3-symmetric deformation and is much stronger. The later is calculated around 1225 cm^{-1} with an IR intensity of about 540 km/mol. As previously seen in structures **2** and **3**, the CH_2 rock of the butyl chain is obtained at about 665 cm^{-1} with a non-negligible IR intensity.

As in the case of structure **1**, the $C_a=O_b$ and $C_b=O_d$ bonds in structure **7** are almost identical and clearly coupled. However, since the acetate groups are not chelated, they appear at much higher frequencies. Surprisingly, the calculated IR intensities of their out-of-phase and in-phase stretching modes are comparable. This is due to the relative orientation of the two CO bonds: while they are almost parallel in structure **1**, the angle between their respective directions is about 72° in structure **7**. The two CH_3-symmetric deformations of the acetate group are also almost identical, resulting in a single out-of-phase mode calculated at 1346 cm^{-1} with an IR intensity of 93 km/mol. Because of the nearly symmetric geometry of the conformer, the stretching motions of the C_a-O_a and C_b-O_c bonds are coupled. However, they have almost the same orientation, resulting in a very weak in-phase stretching mode located at 1225 cm^{-1}. For the same reason, the out-of-phase stretching mode is found to be very intense (1054 km/mol) and is located at 1200 cm^{-1}. Contrary to structure **1**, the acetate CH_3 out-of-phase parallel rock gives rise to a strong band (161 km/mol) situated at 972 cm^{-1}. A careful examination of the vibrational mode reveals that it is slightly coupled to the very intense nearby C_aO_a + C_bO_c out-of-phase stretch, explaining its worth-mentioning intensity. Finally, the CH_2 rock of the butyl chain is predicted at 659 cm^{-1}.

Thus, the main differences between the vibrational characteristics of the located conformers concerns on the one hand the C=O stretching region and on the other hand the 1200−1400 frequency range corresponding to the C_a-O_a and C_b-O_c stretching region either coupled or not with the CH_3-symmetric deformation. Structure **1** generates a single intense band assigned to the C=O stretching mode (the in phase stretch of the terminal C=O bonds) which is lowered in frequency because of the interactions between the tin atom and the oxygen atoms of the carbonyl groups. The calculated IR harmonic frequencies of structures **2** to **6** exhibit two intense bands in the same frequency region corresponding to the uncoupled terminal C=O stretches. In structures **2** and **3**, both of them are perturbed by the interaction with the tin atom while it is more pronounced in the case of the $C_b=O_d$ stretching mode. The same observation can be done for structures **4**, **5**, and **6**, although the $C_a=O_b$ stretch appears at a higher frequency than in structure **2** and **3** and is much more intense than the $C_b=O_d$ stretching mode. In structure **7**, the two stretches (in phase and out of phase) of the terminal C=O bonds are both logically calculated at much higher nearby frequencies.

Structures **2** and **3** are characterized by four detectable bands in the 1200−1400 frequency range, whereas structures **4** to **6** give rise to three noticeable bands in the same region. Because of the symmetry of structures **1** and **7**, only two intense bands are found at such wavenumbers. Nevertheless, these bands being of comparable intensities in structure **1** and significantly different in structure **7**, the two conformers should be unambiguously distinguished.

Finally, the general characteristics of the vibrational spectra of the different conformers of DBTDA in carbon tetrachloride solution are identical to those obtained in the gas phase. As the most stable conformer has a small gas phase calculated dipole moment (0.5 D), the scaled solvent vibrational shifts are only about 10 cm^{-1} for the two bands in the 1650 cm^{-1} region and do not exceed 3 cm^{-1} for the other mentioned bands.

Clearly, including solvent effect with a small dielectric constant such as that of CCl_4 ($\varepsilon = 2.228$) has almost no effect on the relative stability of the different conformers as well as on the molecular structure and the vibrational spectra of DBTDA. This conclusion should still hold with a solvent having

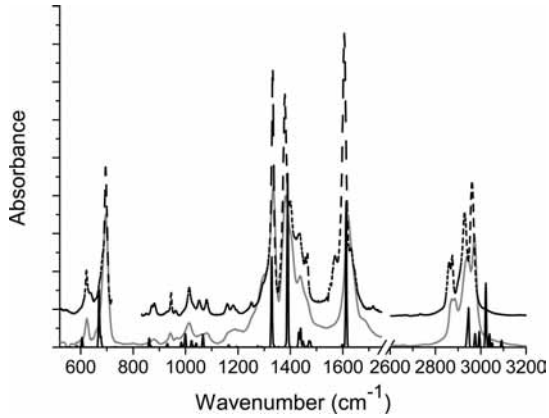

Figure 4. Calculated IR spectra of DBTDA (black solid line). The experimental IR spectra of gaseous DBTDA (gray line) and DBTDA diluted in CCl_4 (1×10^{-2} mol/L) (dashed line) are reported for comparison. The spectrum of DBTDA in CCl_4 has been shifted upward for the clarity of the figure. In addition, the spectral region 700−800 cm^{-1} is not reported for this spectrum because of the strong absorption of CCl_4 in this frequency range.

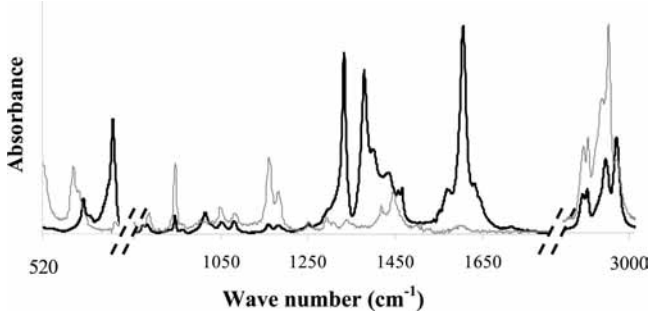

Figure 5. Raman (gray line, 5×10^{-2} mol/L) and IR (black line, 1×10^{-2} mol/L) spectra of DBTDA diluted in CCl_4.

a smaller dielectric constant, such as $scCO_2$ used in our conditions.[41]

4.3. Vibrational Spectra of DBTDA and DBTDL in CCl_4 and $scCO_2$. We have reported in Figure 4 the IR spectrum of DBTDA highly diluted in CCl_4 under ambient conditions compared with that calculated for the conformer **1**. For comparison, we have also reported the experimental spectrum of DBTDA in the gas phase (from the National Institute of Standard and Technology (NIST)).[42] At a first glance, an overall good qualitative and quantitative agreement is observed between the experimental spectra themselves and with the calculated one (Figure 4). Indeed, the fingerprint region of the IR spectrum, namely between 1200 and 1400 cm^{-1}, displays two major peaks of similar intensities located at 1330 and 1380 cm^{-1}. Besides, a single intense band is detected at higher frequency, that is, 1606 cm^{-1}. Let us emphasize that the appearance of a unique band in this spectral region is the specific signature of the conformer **1**, the other conformers showing systematically two peaks of high intensity in this spectral region. We remember that when solvent effects (carbon tetrachloride) were included in the calculations (see earlier), conformer **1** was still the more stable one, its spectrum being almost identical to that calculated in the gas phase. Therefore, as conformer **1** is by far the most representative structure of the overall population of conformers that can be found when DBTDA is highly diluted in CCl_4, the relevant bands observed in the experimental IR and Raman spectra of DBTDA can thus be allocated (see Figure 5 and Table 7). In disagreement with previous reports mentioned above,[14,15] the narrow peak centered at 1606 cm^{-1} in the IR spectrum is assigned to the C═O stretching involving the two carbonyl groups stretching symmetrically (in phase with each other). This mode is barely detected on the Raman spectra, hence confirming that the proposed origin of this peak as the Raman activity of the C═O stretching modes is expected to be weak. The corresponding asymmetric stretching mode of the two carbonyl groups (i.e., out of phase with each other) is in the same frequency range but is postulated to be much weaker than the symmetric component (Table 3). The shoulder on the right-hand side of the IR peak at 1600 cm^{-1} can be tentatively allocated to combinations modes, also detected in the gas phase spectrum, whereas the shoulder on the left-hand side can be explained by the partial bridging of acetoxy group postulated by Okawara et al.[14,15] in concentrated solutions. Indeed, this peak can be observed in the pure liquid phase, whereas it does not appear on the spectrum of DBTDA in the gas phase (Figure 4).[14,15] According to the calculations detailed above, the two relevant peaks centered at 1330 and 1380 cm^{-1} can be assigned to the symmetric "umbrella" deformation modes of methyl groups constituting the acetate moieties, strongly coupled with the out of phase stretching vibrations of the C−O simple bonds. Finally, the peak centered around 690 cm^{-1} can be assigned to the CH_2 rocking modes of the butyl groups. Thus, under catalytic conditions, the most stable configuration for this molecule highly diluted (lower than 5%) in CCl_4 corresponds to the asymmetrically chelated structure (conformer **1**) calculated earlier for the molecule in the gas phase.

TABLE 7: Relevant Frequencies of the IR and Raman Spectrum of DBTDA Diluted in CCl_4 under Ambient Conditions[a]

	IR		Raman	
assignments[b]	frequency (cm^{-1})	intensity	frequency (cm^{-1})	activity
(C_aO_b + C_bO_d) i.p. str	1606	s	1605	w
(CH_2) o. p. def			1445	m
(C_aO_a + C_bO_c) o.p. str + (CH_3) sym. Def	1375	s		
(C_aO_a + C_bO_c) o.p. str. + (CH_3) sym. Def	1315	s		
wagging (CH_2)	1160	w	1161	m
($C-C)_{Ac}$ i.p. str + (O_aSnO_c) def + ($O_aC_aO_b$ + $O_cC_bO_d$) i.p. def	945	w	945	m
rocking (CH_2)	693	s		

[a] s = strong; m = medium; w = weak. [b] i.p. = in phase; o.p. = out of phase; str = stretch; sym = symmetric; def = deformation.

As the DBTDL molecule is much larger than DBTDA, we did not performed DFT calculations on this molecule. Thus, we are not able to probe by molecular modeling the effect of the length of the carbon chain on the structure of these dialkyltin diacetates. However, from the comparison of the IR and Raman spectra of DBTDA and DBTDL, we can postulate if the structure of these two molecules is fundamentally different or not. Thus, in order to check if DBTDL adopts the same asymmetrically chelated structure as DBTDA, we have reported in Figure 6 the IR and Raman spectra of DBTDL diluted in CCl_4 under ambient conditions. As in the case of DBTDA, we observe a single characteristic peak at about 1600 cm^{-1} that can be assigned to the C═O stretching involving the two carbonyl groups stretching symmetrically. As for DBTDA, the Raman activity of this mode is expected to be weak and it is logically barely detected on the Raman spectra. Therefore, from the comparison between the vibrational spectra of DBTDA and DBTDL, we can postulate unambiguously that DBTDL diluted in CCl_4 adopts the same asymmetrically chelated structure as DBTDA.

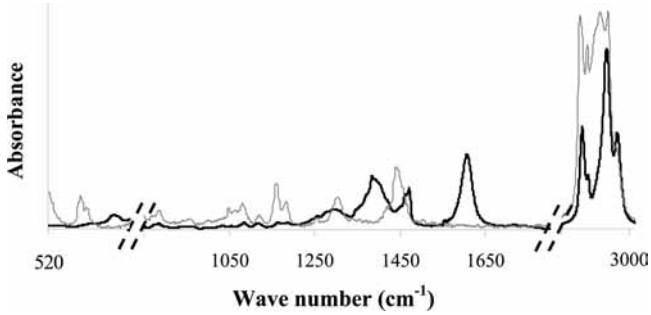

Figure 6. Raman (gray line, 5×10^{-2} mol/L) and IR (black line, 1×10^{-2} mol/L) spectra of DBTDL diluted in CCl_4 (1×10^{-2} mol/L).

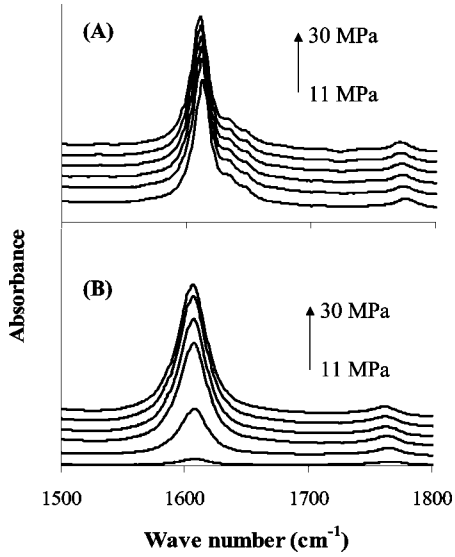

Figure 7. IR spectra of O═C−O vibration modes of DBTDA (A) and DBTDL (B) at 1×10^{-3} mol·L^{-1} in CO_2 at different pressures (11, 13, 16, 20, 25, and 30 MPa) and constant temperature (60 °C).

We then performed mid-infrared absorption (IR) measurements on DBTDA and DBTDL highly diluted in $scCO_2$. We were not able to report the Raman spectra under the same conditions because of the low solubility ($<10^{-3}$ mol·l^{-1}) of these organotin compounds in $scCO_2$. To probe the effect of the density of $scCO_2$ on the structure of these dialkytin diacetates, we have collected the IR spectra in the C═O stretching region of DBTDA and DBTDL in $scCO_2$ at 60 °C as a function of pressure (Figure 7). Whatever the pressure is, the IR spectra display a single intense band centered at about 1620 cm^{-1} for DBTDA, and at 1610 cm^{-1} for DBTDL, that can be assigned to the C═O in-phase stretching mode.

Therefore, as found in the case of CCl_4, the experimental spectrum of DBTDA in $scCO_2$ is particularly in good qualitative and quantitative agreement with that calculated for the conformer **1**. Also, from the comparison between the vibrational spectra of DBTDA and DBTDL in $scCO_2$, we can confirm that DBTDL diluted in $scCO_2$ adopts the same asymmetrically chelated structure as DBTDA.

In addition, a weak shift of about 3 and 2 cm^{-1} for DBTDA and DBTDL, respectively, is detected as a function of pressure and might result from weak EDA interactions occurring between the C═O groups of both dialkytin diacetates and CO_2. Such type of interaction has been already reported for organic molecules or polymers containing carbonyl groups, CO_2 acting as a Lewis acid favoring the formation of electron donor−acceptor (EDA) complexes.[43−46]

The weak peak at about 1760 cm^{-1} detected in the IR spectra of DBTDA and DBTDL is assigned to the C═O stretching

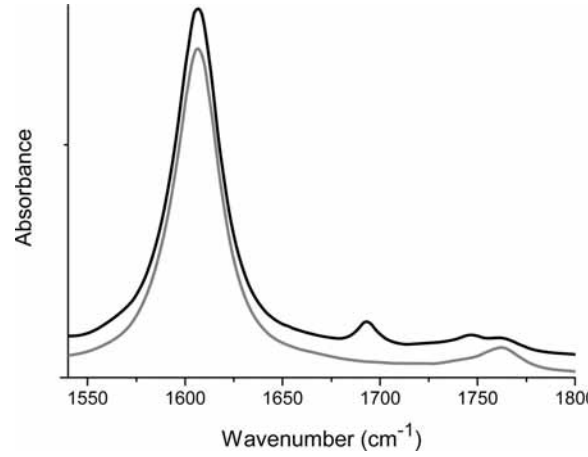

Figure 8. IR spectra of O═C−O vibration modes of DBTDL (1×10^{-3} mol/L) in CO_2 (30 MPa, 60 °C) 10 min after addition of CO_2 (gray) and 20 h after addition of CO_2 (black).

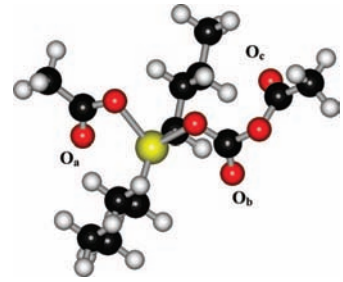

Figure 9. Optimized geometry at the B3LYP/DGDZVP level of DBTDA where one CO_2 molecule has been inserted in one Sn−O bond.

modes of the corresponding acetic and lauric acids. Their presence in dense CO_2 is due to the partial hydrolysis of DBTDA and DBTDL.[15,47]

Finally, to check that DBTDL and DBTDA were not subject over time to major side reactions in $scCO_2$, we have measured the IR spectrum of both catalysts in $scCO_2$ at 60 °C and 30 MPa as a function of time. The IR spectrum of DBTDL recorded 20 h after the addition of CO_2 is compared with that measured only 10 min after CO_2 addition (Figure 8). The main peak at 1600 cm^{-1} is observed in both spectra showing that DBTDL is stable in $scCO_2$. However, we can observe two new weak peaks centered at about 1690 and 1750 cm^{-1} that appear in the spectrum measured 20 h after addition of CO_2. The same observation has been done in the case of DBTDA for which two new weak peaks centered at about 1720 and 1770 cm^{-1} emerge in the spectrum over a similar period of time.

The appearance of these two new peaks may result from the insertion of CO_2 in the Sn−O bond as reported by previous authors[26] on tin alkoxyde. To ensure the assignment of these new bands, we have performed DFT calculations on a DBTDA molecule where one CO_2 molecule has been inserted in one Sn−O bond of DBTDA (see Figure 9). The calculations have been performed using the same level of theory as that used for DBTDA. The spectrum of such a molecule displays three peaks in the C═O stretching region, centered at 1564, 1685, and 1752 cm^{-1} associated to the C═O stretch of C═O_a, C═O_b, and C═O_c, respectively. If we compare these frequencies to that observed on the IR spectrum of DBTDA and DBTDL, we can assign the two peaks observed in the experimental spectra at about 1700 and 1750 cm^{-1} to the C═O_b and C═O_c mode of vibration which results from the insertion of CO_2 in one Sn−O bond. The third vibrational mode (1564 cm^{-1}) is not detected

as it would appear in the same frequency region as the main peak at 1600 cm^{-1} observed for both catalysts. Therefore, the spectral modifications observed as a function of time are related to the insertion of CO_2 in the Sn−O bond. Thus, it appears that these diorganotin dicarboxylate compounds react slightly with $scCO_2$. However, such a reaction is relatively slow and it can reasonably be postulated that the activity of DBTDL and DBTDA in $scCO_2$ should remain during the earliest stage of the polymerization. This result is supported by our previous work on the synthesis of polyurethane particles in $scCO_2$,[22] showing that the presence of DBTDL enhances drastically the reactivity between the diol and the isocyanate and allows us to obtain high molecular weight polyurethane materials.

5. Conclusion

The DBTDA molecule was modeled using density functional theory. Different conformers have been investigated and the obtained relative energies appear directly connected to the orientation of the final oxygen atoms of the acetate group with respect to the tin atom. Thus, because of the Sn···O interactions, the lowest energy conformer reveals an asymmetrically chelated structure of the acetate groups with a C_{2v} symmetry. The experimental IR spectrum of the molecule diluted in carbon tetrachloride and in $scCO_2$ corroborates this conformation. Moreover, the experimental IR spectrum of the DBTDL, carried out under the same conditions, is highly comparable, indicating that DBTDL adopts in CCl_4 and $scCO_2$ an asymmetrically chelated structure as found for DBTDA. A new attribution of the relevant bands constituting the IR spectrum of the catalysts could be carried out. Finally, the catalysts diluted in $scCO_2$ were investigated as a function of time. Although both species react slightly with $scCO_2$, their spectrum remains unchanged during the first hours. The molecules thus preserve a priori a catalytic activity similar to that noted in conventional organic solvent.

Acknowledgment. We gratefully acknowledge computational facilities provided by the computers of the M3PEC-Mesocentre, DRIMM- University Bordeaux 1 (http://www.m3pec.u-bordeaux1.fr), financed by the "Conseil Regional d'Aquitaine" and the French Ministry of Research and Technology. B. Renault acknowledges the Region Aquitaine and CNRS for fellowship.

References and Notes

(1) Bayer, O. A process for the production of polyurethanes and polyureas, German Patent DRP 728981, (1937).
(2) Silva, A. L.; Bordalo, J. C. *Catal. Rev.* **2004**, *46*, 31.
(3) Draye, A. C.; Tondeur, J. J. *J. Mol. Catal. A* **1999**, *138*, 135.
(4) Draye, A. C.; Tondeur, J. J. *J. Mol. Catal. A* **1999**, *140*, 31.
(5) Ent'yelees, S. G.; N'Yest'yerov, O. V.; Zabrodeen, V. B. *J. Catal.* **1967**, *7*, 309.
(6) Ent'yelees, S. G.; N'Yest'yerov, O. V. *J. Catal.* **1967**, *7*, 202.
(7) Houghton, R. P.; Mulvaney, A. W. *J. Organomet. Chem.* **1996**, *518*, 21.
(8) Lipatova, T. E.; Bakalo, L. A.; Niselsky, N. Y.; Sirotinskaya, A. L. *J. Macromol. Sci-Chem* **1970**, *A4*, 1743.
(9) Luo, S. G.; Tan, H. M.; Zhang, J. G.; Wu, Y. J.; Pei, F. K.; Meng, X. H. *J. Appl. Polym. Sci.* **1997**, *65*, 1217.
(10) Majumdar, K. K.; Kundu, A.; Das, I.; Roy, S. *Appl. Organomet. Chem.* **2000**, *14*, 79.
(11) Smith, H. A. *J. Appl. Polym. Sci.* **1963**, *7*, 85.
(12) Van der Weij, F. W. *J. Polym. Sci.* **1981**, *19*, 381.
(13) Cahours, A. *Ann. Chem.* **1860**, *114*, 354.
(14) Maeda, Y.; Okawara, R. *J. Organomet. Chem.* **1967**, *10*, 247.
(15) Okawara, R.; Ohara, M. Organotin compounds with Sn-O bonds. Organotin carboxylates, salts, and complexes. In *Organotin Compounds*; Sawyer, A. K., Ed.; Marcel Dekker: New York, 1971; Vol. 2, pp 253.
(16) Tiekink, R. T. E. *Appl. Organometal. Chem.* **1991**, *5*, 1.
(17) Pettinari, C. *J. Organomet. Chem.* **2006**, *691*, 1435.
(18) Jankovics, H.; Pettinari, C.; Marchetti, F.; Kamu, E.; Nagy, L.; Troyanov, S.; Pellerito, L. *J. Inorg. Biochem.* **2003**, *97*, 370.
(19) Khan, M. I.; Baloch, M. K.; Ashfaq, M.; Peters, G. J. *Appl. Organomet. Chem.* **2005**, *19*, 132.
(20) Szorcsik, A.; Nagy, L.; Pellerito, L.; Lampeka, R. D. *J. Radioanal. Nucl. Chem.* **2003**, *257*, 285.
(21) Yin, H.-D.; Wang, Q.-B.; Xue, S.-C. *J. Organomet. Chem.* **2004**, *689*, 2480.
(22) Renault, B.; Tassaing, T.; Cloutet, E.; Cramail, H. *J. Polym. Sci., Part A* **2007**, *45*, 5649.
(23) Chambon, P.; Cloutet, E.; Cramail, H. *Macromolecules* **2004**, *37*, 5856.
(24) Chambon, P.; Cloutet, E.; Cramail, H.; Tassaing, T.; Besnard, M. *Polymer* **2005**, *46*, 1057.
(25) Renault, B.; Cloutet, E.; Cramail, H.; Tassaing, T.; Besnard, M. *J. Phys. Chem. A* **2007**, *111*, 4181.
(26) Stassin, F.; Halleux, O.; Jérôme, R. *Macromolecules* **2001**, *34*, 775.
(27) Bergeot, V.; Tassaing, T.; Besnard, M.; Cansell, F.; Mingotaud, A.-F. *J. Supercrit. Fluids* **2004**, *28*, 249.
(28) Lalanne, P.; Tassaing, T.; Danten, Y.; Cansell, F.; Tucker, S. C.; Besnard, M. *J. Phys. Chem. A* **2004**, *108*, 2617.
(29) Frisch, M. J.; Trucks, G. W.; Schlegel, H. B.; Scuseria, G. E.; Robb, M. A.; Cheeseman, J. R.; Montgomery, Jr J. A. T. V.; Kudin, K. N.; Burant, J. C.; Millam, J. M.; Iyengar, S. S.; Tomasi, J.; Barone, V.; Mennucci, B.; Cossi, M.; Scalmani, G.; Rega, N.; Petersson, G. A.; Nakatsuji, H.; Hada, M.; Ehara, M.; Toyota, K.; Fukuda, R.; Hasegawa, J.; Ishida, M.; Nakajima, T.; Honda, Y.; Kitao, O.; Nakai, H.; Klene, M.; Li, X.; Knox, J. E.; Hratchian, H. P.; Cross, J. B.; Bakken, V.; Adamo, C.; Jaramillo, J.; Gomperts, R.; Stratmann, R. E.; Yazyev, O.; Austin, A. J.; Cammi, R.; Pomelli, C. ; Ochterski, J. W.; Ayala, P. Y.; Morokuma, K.; Voth, G. A.; Salvador, P.; Dannenberg, J. J.; Zakrzewski, V. G.; Dapprich, S.; Daniels, A. D.; Strain, M. C.; Farkas, O.; Malick, D. K.; Rabuck, A. D.; Raghavachari, K.; Foresman, J. B.; Ortiz, J. V.; Cui, Q.; Baboul, A. G.; Clifford, S.; Cioslowski, J.; Stefanov, B. B.; Liu, G.; Liashenko, A.; Piskorz, P.; Komaromi, I.; Martin, R. L.; Fox, D. J.; Keith, T.; Al.Laham, M. A.; Peng, C. Y.; Nanayakkara, A.; Challacombe, M.; Gill, P. M. W.; Johnson, B.; Chen, W.; Wong, M. W.; Gonzalez, C.; Pople, J. A. *Gaussian 03*, revision C.02; Gaussian, Inc.: Wallingford, CT, 2004.
(30) Becke, A. D. *J. Chem. Phys.* **1993**, *98*, 5648.
(31) Lee, C.; Yang, W.; Parr, R. G. *Phys. Rev. B* **1988**, *37*, 785.
(32) Stephens, P. J.; Devlin, F. J.; Chabalowski, C. F.; Frisch, M. J. *J. Phys. Chem.* **1994**, *98*, 11623.
(33) Godbour, N.; Salahub, D. R.; Andzelm, J.; Wimmer, E. *Can. J. Chem.* **1992**, *70*, 560.
(34) Sosa, C.; Andzelm, J.; Elkin, B. C.; Wimmer, E.; Dobbs, K. D.; Dixon, D. A. *J. Phys. Chem.* **1992**, *96*, 6630.
(35) Schaftenaar, G.; Noordik, J. H. *J. Comput.-Aided Mol. Des.* **2000**, *14*, 123.
(36) Scott, A. P.; Radom, L. *J. Phys. Chem.* **1996**, *100*, 16502.
(37) Irikura, K. K.; Johnson, R. D.; Kacker, R. N. *J. Phys. Chem. A* **2005**, *109*, 8430.
(38) Barone, V.; Cossi, M.; Tomasi, J. *J. Comput. Chem.* **1998**, *19*, 404.
(39) Amovilli, C.; Barone, V.; Cammi, R.; Cances, E.; Cossi, M.; Mennucci, B.; Pomelli, C. S.; Tomasi, J. Quantum Systems in Chemistry and Physics, Part II. In *Advanced Quantum Chemistry*; Academic Press Inc: San Diego, CA, 1999; Vol. 32.
(40) Tomasi, J.; Mennucci, B.; Cammi, R. *Chem. Rev.* **2005**, *105*, 2999.
(41) Moriyoshi, T.; Kita, T.; Uosaki, Y. *Ber. Bunsenges. Phys. Chem* **1993**, *97*, 589.
(42) http://webbook.nist.gov/chemistry/ Accessed June, 2007.
(43) Kazarian, S. G.; Vincent, M. F.; Bright, F. V.; Liotta, C. L.; Eckert, C. A. *J. Am. Chem. Soc.* **1996**, *118*, 1729.
(44) Nelson, M. R.; Borkman, R. F. *J. Phys. Chem. A* **1998**, *102*, 7860.
(45) Raveendran, P.; Wallen, S. L. *J. Am. Chem. Soc.* **2002**, *124*, 12590.
(46) Jamroz, M. H.; Dobrowolski, J. C.; Bajdor, K.; Borowiak, M. A. *J. Mol. Struct.* **1995**, *349*, 9.
(47) Palmlöf, M.; Hjertberg, T. *J. Appl. Polym. Sci.* **1998**, *72*, 521.

JP8004822